PHYSICAL REVIEW D **88,** 074015 (2013)

Probing the nature of the Higgs-gluon coupling

Robert V. Harlander* and Tobias Neumann†

Bergische Universität Wuppertal, 42097 Wuppertal, Germany

(Received 14 August 2013; published 15 October 2013)

One- and two-jet observables of dimension-7 Higgs-gluon coupling operators are studied as probes of possible deviations from the top-loop induced gluon-Higgs coupling. We discuss the case of both a scalar as well as a pseudoscalar Higgs boson and show that higher order operators can give visible deviations from Standard Model distribution shapes.

DOI: 10.1103/PhysRevD.88.074015 PACS numbers: 12.38.Bx, 12.60.Fr, 12.38.−t

I. INTRODUCTION

The mechanism of electroweak symmetry breaking is in its phase of identification. The recent discovery [1,2] of a Higgs boson at the Large Hadron Collider (LHC) provides a new probe for physics beyond the Standard Model (SM) through precision physics. Up to now, the signals are in very good agreement with SM predictions, but there is still room for traces of an extended theory.

The production and decay rates of the SM Higgs boson have been predicted by higher order theoretical calculations (see Refs. [3–5]). The dominant production mechanism is through gluon fusion, where the coupling of the gluons to the Higgs boson is mediated predominantly by a top-quark loop. It should be one of the main goals of the LHC to test the character of this gluon-Higgs coupling.

The loop-induced coupling differs particularly strongly from a pointlike vertex if an external mass scale of the process becomes larger than the top-quark mass, and thus allows one to resolve the nontrivial structure of the Higgs-gluon vertex. This suggests looking at processes involving large transverse momenta of the Higgs boson or an associated jet, for example, and compare the SM prediction with a pointlike coupling.

A general description of a pointlike gluon-Higgs coupling that is compatible with the gauge symmetries of the SM can be obtained in terms of an effective theory. The leading operator for a scalar Higgs, $\mathcal{O}_1 = HF^a_{\mu\nu}F^{a,\mu\nu}$ is of mass dimension 5. In the limit of an infinite top mass, $m_t \to \infty$, and neglecting the Yukawa coupling of lighter quarks, the SM gluon-Higgs coupling reduces to this single operator; for finite m_t, it allows for a reasonable approximation of the SM gluon-Higgs coupling and is typically used for evaluating perturbative correction factors to the SM cross section prediction. Differential cross sections based on $\mathcal{O}_1$ have therefore been studied quite extensively. The purpose of our paper is to see the effect of higher dimensional operators on the most important kinematical distributions. These operators of mass dimension 7 are well known; they will be recalled in the next section.

*robert.harlander@uni-wuppertal.de
†tobias.neumann@uni-wuppertal.de

The philosophy of our analysis is therefore as follows: assume that it turns out that the gluon-Higgs coupling is *not* (or not mainly) induced by a top-quark loop as in the SM, but by pointlike vertices generated by some new physics at a higher scale. The coupling strengths of the effective operators (at least one of them) has to be SM-like in order to account for the signal strength observed experimentally. It will then be important to consider kinematical distributions of the Higgs boson and the associated jets and compare them with the predictions based on the effective Lagrangian to be introduced below. Our analysis includes the production of both scalar and pseudoscalar Higgs bosons (both denoted as H in what follows) and will be based on $H + 1$- and $H + 2$-jet observables. For similar, though more model-specific analyses, see Refs. [6–9], for example.

Note that since we assume that gluon fusion is the dominant Higgs production mechanism at the LHC, we do not need to take into account the full set of effective operators as defined in Refs. [10,11]. Rather, we can restrict ourselves to operators involving only gluons, quarks, and the Higgs field. Operators constructed from electroweak fields typically affect the branching ratios of the Higgs boson; a comprehensive list of references for studies in this direction can be found in Refs. [3,12].

The remainder of this paper is organized as follows. In Sec. II, the basis of dimension-5 and -7 operators is recalled that couple a scalar or a pseudoscalar particle to gluons in a gauge invariant way. We also briefly describe some technical issues of our study. Section III presents distributions of $H + 1$-jet and $H + 2$-jets observables as induced by the formally leading and subleading terms in the effective theory. The SM case is reproduced for comparison. In Sec. IV, we also consider terms that are formally suppressed by higher powers of the "new physics scale" Λ, which occurs in the effective theory. In Sec. V we present our conclusions.

II. BASIS OF DIMENSION-7 OPERATORS AND THEIR IMPLEMENTATION

This section describes the operator basis used in our calculation. We start with the effective Lagrangian for the coupling of a scalar boson to gluons and generalize

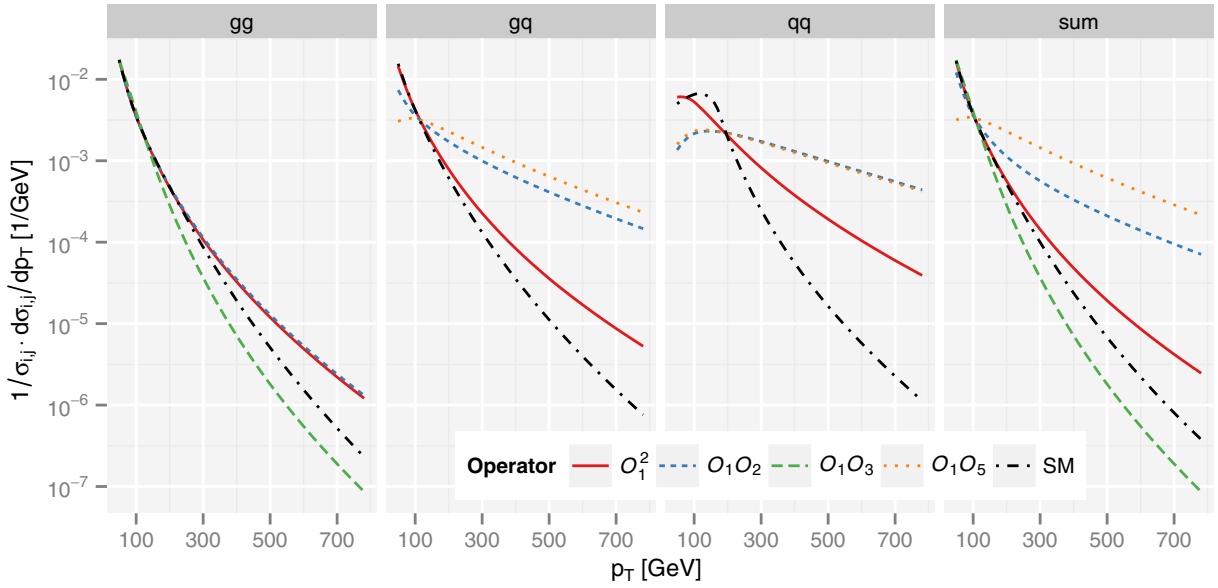

FIG. 1 (color online). Normalized Higgs transverse momentum distributions for scalar coupling operators. The normalization factors σ_{ij} are given in Table I.

the discussion to pseudoscalar bosons in the subsequent section.

A. Scalar Higgs boson

The effective Lagrangian involving operators through mass dimension 7 that couple a scalar Higgs boson H to gluons can be written as [13,14] (see also Ref. [15])

$$\mathcal{L} = \frac{C_1}{\Lambda}\mathcal{O}_1 + \sum_{n=2}^{5}\frac{C_n}{\Lambda^3}\mathcal{O}_n, \tag{1}$$

$$\begin{aligned}
&\mathcal{O}_1 = HF^a_{\mu\nu}F^{a\mu\nu}, \qquad \mathcal{O}_2 = HD_\alpha F^a_{\mu\nu}D^\alpha F^{a\mu\nu},\\
&\mathcal{O}_3 = HF^{a\mu}_{\nu}F^{b\nu}_{\sigma}F^{c\sigma}_{\mu}f^{abc}, \qquad \mathcal{O}_4 = HD^\alpha F^a_{\alpha\nu}D_\beta F^{a\beta\nu},\\
&\mathcal{O}_5 = HF^a_{\alpha\nu}D^\nu D^\beta F^{a\alpha}_{\beta},
\end{aligned} \tag{2}$$

where

$$\begin{aligned}
F^a_{\mu\nu} &= \partial_\mu A^a_\nu - \partial_\nu A^a_\mu - g_s f^{abc}A^b_\mu A^c_\nu,\\
D_\mu A^a_\nu &= \partial_\mu A^a_\nu - g_s f^{abc}A^b_\mu A^c_\nu,
\end{aligned} \tag{3}$$

with the gluon field A^a_μ. The strong coupling is denoted by g_s, and f^{abc} are the SU(3) structure constants. We remark that, for an on-shell Higgs boson, the operators in Eq. (2) are not linearly independent. Instead, one finds $m_H^2\mathcal{O}_1 = 4\mathcal{O}_5 - 2\mathcal{O}_2 + 4g_s\mathcal{O}_3$, where m_H is the Higgs mass, and thus one of $\mathcal{O}_2$, $\mathcal{O}_3$, and $\mathcal{O}_5$ could be eliminated from our analysis. Nevertheless, we find the basis in Eq. (2) convenient and therefore stick to this redundancy.

The mass parameter Λ in Eq. (1) is undetermined *a priori*; in the SM, it is the top-quark mass m_t, for example. Matching the effective Lagrangian of Eq. (1) to the SM allows one to derive perturbative expressions C_i^{SM} for the Wilson coefficients C_i. For example, C_1^{SM} is known through $\mathcal{O}(\alpha_s^5)$ [16,17]; explicit expressions for the C_n^{SM} ($n \in \{2,\ldots,5\}$), on the other hand, have been obtained only at next-to-leading order (NLO) [14], where we give the leading order (LO) expressions as follows[1]:

$$\begin{aligned}
C_1^{\mathrm{SM}} &= \frac{g_s^2\lambda_t}{48\pi^2} + \mathcal{O}(g_s^4) \simeq 2.2\times 10^{-3},\\
C_2^{\mathrm{SM}} &= \frac{-7g_s^2\lambda_t}{2880\pi^2} + \mathcal{O}(g_s^4) \simeq -2.6\times 10^{-4},\\
C_3^{\mathrm{SM}} &= -\frac{g_s^3\lambda_t}{240\pi^2} + \mathcal{O}(g_s^5) \simeq -5.3\times 10^{-4},\\
C_4^{\mathrm{SM}} &= \frac{g_s^2\lambda_t}{1440\pi^2} + \mathcal{O}(g_s^4) \simeq 7.3\times 10^{-5},\\
C_5^{\mathrm{SM}} &= \frac{g_s^2\lambda_t}{80\pi^2} + \mathcal{O}(g_s^4) \simeq 1.3\times 10^{-3},
\end{aligned} \tag{4}$$

where $\lambda_t = m_t/v$ is the top-quark Yukawa coupling, and the values $m_t = 172$ GeV, $v = 246$ GeV, and $g_s = \sqrt{4\pi\alpha_s}$, with $\alpha_s = 0.118$, have been inserted in order to arrive at a numerical illustration for the size of these coefficients.

Nominally, contributions of $\mathcal{O}_1$ are suppressed by $1/\Lambda^2$ in physical quantities, mixed terms of $\mathcal{O}_1$ with $\mathcal{O}_2$ to $\mathcal{O}_5$ are suppressed by $1/\Lambda^4$, etc. Note, however, that in the SM, the matching coefficients are proportional to $\lambda_t \sim m_t/v = \Lambda/v$. This cancels the prefactor $1/\Lambda$ in Eq. (1) and thus the overall suppression. Since we want to keep the discussion as general as possible, we will mostly ignore the suppression of the higher dimensional operators; all that

[1]Reference [14] misses a factor of $-3/4$ in C_3^{SM}, at least at LO, which we correct here.

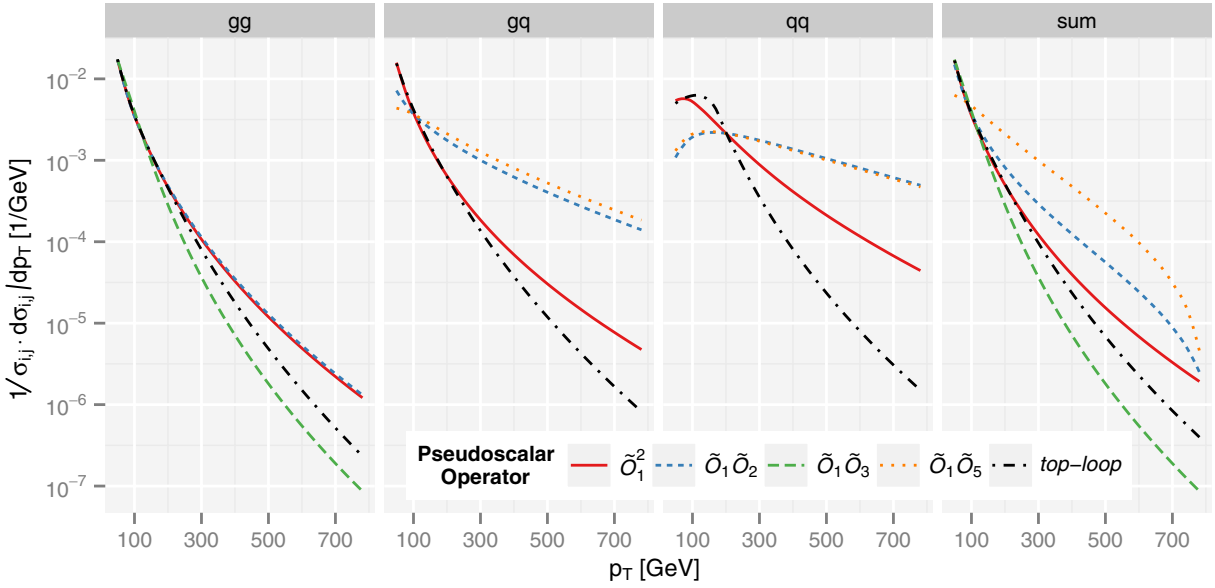

FIG. 2 (color online). Same as Fig. 1, but for pseudoscalar coupling operators. Note that the gg channel is identical to the scalar case. The σ_{ij} are given in Table II.

is relevant to us is the influence of the individual operators on the shape of the distributions.

a. Remark on operators containing quark fields. The operators $\mathcal{O}_4$ and $\mathcal{O}_5$ can be rewritten as operators containing two and one quark bilinears according to the QCD equations of motion [18–20]:

$$D^\mu F^a_{\mu\nu}(x) = g_s \bar{\Psi}(x)\gamma_\nu t^a \Psi(x). \tag{5}$$

In case of gluodynamics, these two operators then vanish [13]. They contribute only when their corresponding quark representation can occur in the given process/Feynman diagrams.

B. Pseudoscalar Higgs boson

In addition to the production of a scalar Higgs boson, we also consider the pseudoscalar analogue that, for the sake of simplicity, we also denote by H in this paper.[2] The corresponding effective operators are obtained from the scalar case by replacing one of the field strength tensors by its dual $\tilde{F}^a_{\mu\nu} = \frac{1}{2}\epsilon_{\mu\nu\rho\sigma}F^{a\rho\sigma}$, with the Levi-Cività symbol $\epsilon_{\mu\nu\rho\sigma}$. We therefore obtain

$$\mathcal{L} = \frac{\tilde{C}_1}{\Lambda}\mathcal{O}_1 + \sum_{n=2}^{5}\frac{\tilde{C}_n}{\Lambda^3}\mathcal{O}_n, \tag{6}$$

$$\begin{aligned}
\tilde{\mathcal{O}}_1 &= H\tilde{F}^a_{\mu\nu}F^{a\mu\nu}, \qquad \tilde{\mathcal{O}}_2 = HD_\alpha\tilde{F}^a_{\mu\nu}D^\alpha F^{a\mu\nu},\\
\tilde{\mathcal{O}}_3 &= H\tilde{F}^{a\mu}_{\nu}F^{b\nu}_{\sigma}F^{c\sigma}_{\mu}f^{abc}, \qquad \tilde{\mathcal{O}}_4 = HD^\alpha\tilde{F}^a_{\alpha\nu}D_\beta F^{a\beta\nu},\\
\tilde{\mathcal{O}}_5 &= H\tilde{F}^a_{\alpha\nu}D^\nu D^\beta F^{a\alpha}_{\beta}.
\end{aligned} \tag{7}$$

[2]It should be clear from the context whether H denotes the scalar or the pseudoscalar Higgs boson.

We generated the Feynman rules for the operators $\mathcal{O}_n$ and $\tilde{\mathcal{O}}_n$ ($n = 1, \ldots, 5$) using LanHEP [21] and confirmed their validity with FeynRules [22]. A nonzero contribution of the operator $\tilde{\mathcal{O}}_4$ involves at least six gluons; therefore, it does not appear in our numerical analysis below. Furthermore, similar to the scalar case, the remaining operators are not linearly independent for an on-shell Higgs boson, but for convenience we will include all of them in our analysis.

TABLE I. Normalization factors for p_T distributions in H + 1-jet production for a scalar Higgs. They are obtained by integrating the distributions of Fig. 1 over the interval $p_T \in [30, 800]$ GeV.

	σ_{ij}/pb for H + 1-jet (scalar)		
ij	gg	gq	qq
SM/α_s^2	4.79×10^2	1.78×10^2	3.13
11	3.88×10^{10}	1.59×10^{10}	1.03×10^8
12	-5.55×10^{14}	-6.59×10^{14}	3.05×10^{13}
13	-2.00×10^{13}	⋯	⋯
15	⋯	-2.05×10^{14}	1.60×10^{13}

TABLE II. Same as Table I, but for a pseudoscalar Higgs (see Fig. 2).

	σ_{ij}/pb for H + 1-jet (pseudoscalar)		
ij	gg	gq	qq
Top-loop/α_s^2	1.11×10^3	4.16×10^2	6.67
11	3.88×10^{10}	5.06×10^9	3.13×10^8
12	-5.56×10^{14}	-3.22×10^{14}	8.87×10^{13}
13	-2.00×10^{13}	⋯	⋯
15	⋯	-1.21×10^{14}	4.68×10^{13}

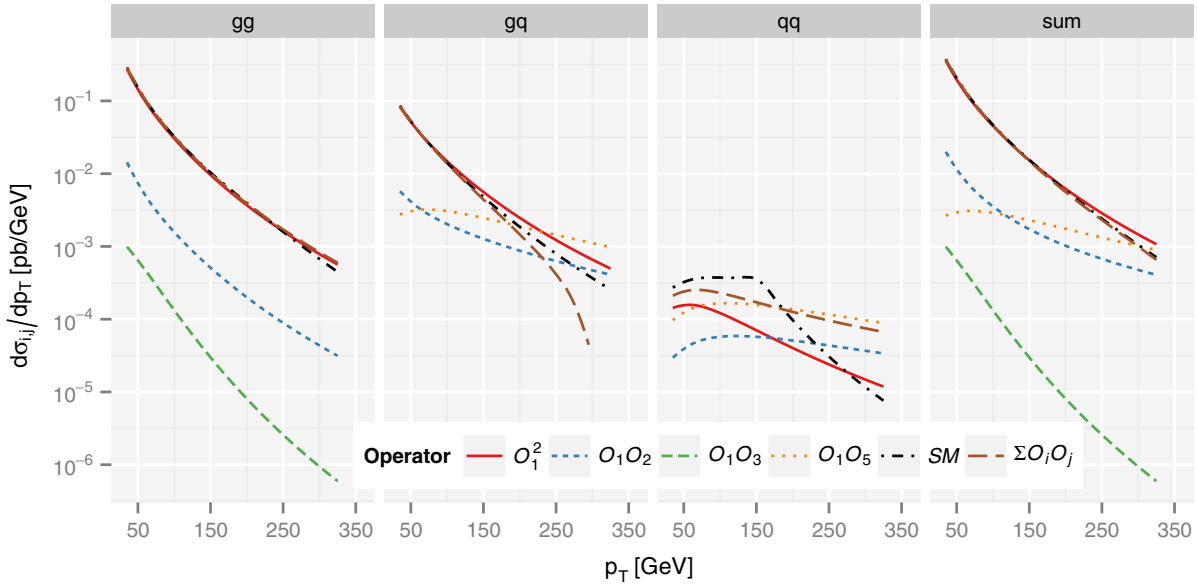

FIG. 3 (color online). Higgs transverse momentum distributions with SM matching coefficients, resulting in a total m_t^2 suppression with respect to C_1^2. Note that in the case of the gq and summed channel the cross term $\mathcal{O}_1\mathcal{O}_5$ has been multiplied with -1. For the qq channel the cross term $\mathcal{O}_1\mathcal{O}_2$ has been multiplied with -1.

With the obtained vertices, the necessary LO Feynman graphs for H + 1-jet and H + 2-jet amplitudes were generated with DIANA [23] as FORM [24] code. The analytical expressions for the matrix elements were then calculated by inserting the Feynman rules, where we used the Feynman gauge and Faddeev-Popov ghosts, as well as an axial gauge for cross-checking. The calculation of the cross sections was performed by means of standard VEGAS integration.

The operator $\tilde{\mathcal{O}}_4$ only contributes at higher order or in 3-jet production. This can easily be seen by switching to the quark representation using QCD equations of motion. The only nonvanishing Feynman-vertex contribution contains three gluons and a quark-antiquark pair; thus it does not appear in the quantities considered in this paper at LO. All lower order vertices vanish due to the contraction of equal-momentum vectors with the Levi-Cività symbol.

III. KINEMATICAL DISTRIBUTIONS

In what follows, we consider the transverse momentum distribution of the Higgs boson when it is produced in

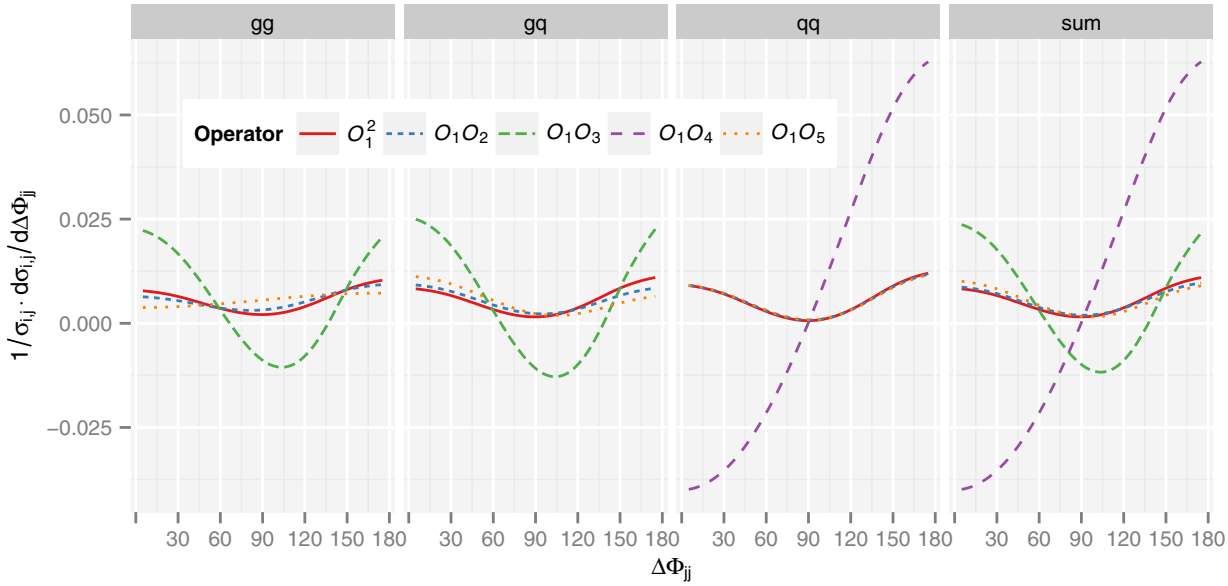

FIG. 4 (color online). Normalized distributions for azimuthal angle difference of the two final state jets for scalar operators. The σ_{ij} are given in Table III.

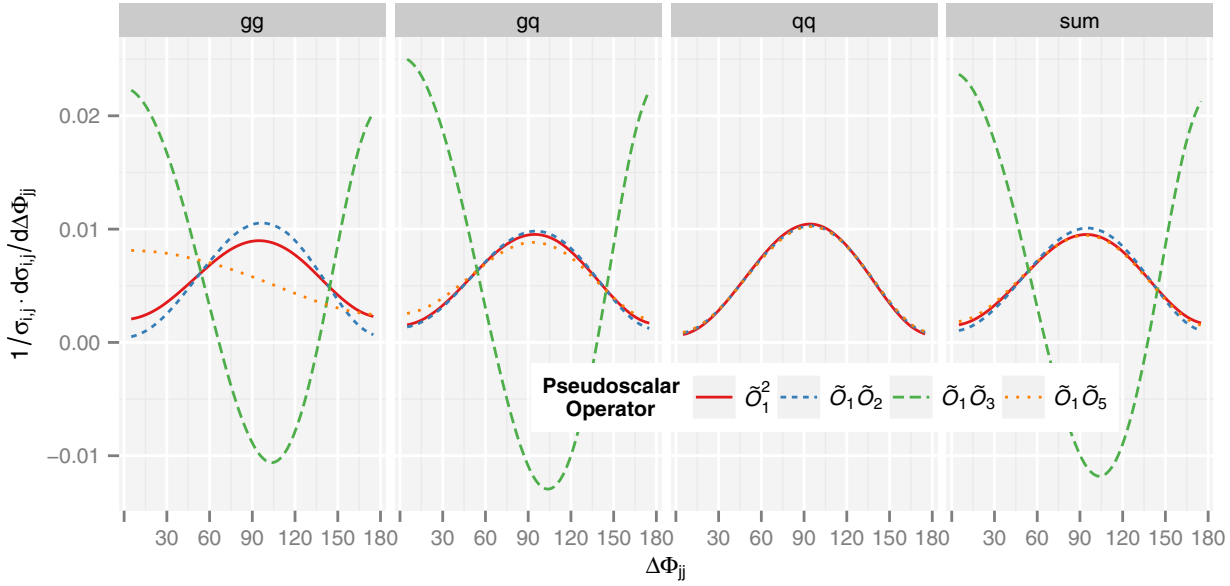

FIG. 5 (color online). Same as Fig. 4, but for pseudoscalar operators. The σ_{ij} are given in Table IV.

association with one or two jets, H + 1-jet and H + 2-jet for short. In the H + 1-jet case, we compare the distributions obtained for the pointlike vertices $\mathcal{O}_n$ and $\tilde{\mathcal{O}}_n$ ($n = 1, \ldots, 5$) with the SM-like loop-induced coupling.

The differential cross section based on the Lagrangian of Eq. (1) can be written as

$$d\sigma = \sum_{i,j=1}^{5} d\sigma_{ij}, \tag{8}$$

where $d\sigma_{ij}$ is due to terms of the form $\mathcal{O}_i\mathcal{O}_j^\dagger$. To be independent of the actual size of the Wilson coefficients, we consider kinematical distributions normalized to their respective contribution to the inclusive cross section σ_{ij}, i.e., $d\sigma_{ij}/\sigma_{ij}$. Absolute effects on the distributions within a given model, i.e., for concrete values of the Wilson coefficients C_i and the "new physics scale" Λ, can be derived by combining these normalized distributions with the numerical values for the total cross sections σ_{ij} provided in Appendix . Notice that interference terms with $i \neq j$ need not be positive definite.

TABLE III. Normalization factors for $\Delta\Phi_{jj}$ distributions in H + 2-jet production for a scalar Higgs. They are obtained by integrating the distributions of Fig. 4 over the interval $\Delta\Phi_{jj} \in [0, \pi]$, with the cuts described in Eqs. (9) and (10).

	σ_{ij}/pb for H + 2-jet (scalar), WBF cuts		
ij	gg	gq	qq
11	1.43×10^9	2.27×10^9	8.42×10^8
12	-2.14×10^{13}	-6.54×10^{13}	-4.47×10^{13}
13	-7.13×10^{11}	-7.59×10^{11}	$\cdots$
14	$\cdots$	$\cdots$	-1.19×10^{12}
15	-4.65×10^{11}	-1.60×10^{13}	-1.58×10^{13}

We will show distributions for LHC proton-proton collisions, split into the partonic gluon-gluon (gg), the gluon-quark (gq), and quark-quark (qq) initial states (qq includes quark-antiquark as well as different-flavor initial states). At LO, the operator $\mathcal{O}_5$ contributes only to the gq channel because, according to Eq. (5), it can be rewritten to include a quark bilinear term. Analogously, $\mathcal{O}_4$ can be rewritten to contain two quark bilinears, and therefore only contributes to the qq channel. For the gq channel, $\mathcal{O}_3$ does not contribute because its Feynman rules involve at least three gluons.

All distributions are generated for a Higgs mass of $m_H = 125$ GeV and a center of mass energy of $\sqrt{s} = 13$ TeV. For the H + 1-jet p_T distributions, the choice of factorization and renormalization scale is $\mu = \sqrt{m_H^2 + p_T^2}$ and in the case of H + 2-jet cross sections the jet-p_T geometric mean $\mu = \sqrt{p_T(j_1)p_T(j_2)}$. Because of our normalization, the results are largely unaffected by changes of m_H and $\sqrt{s}$.

A. H + 1-jet cross sections

First we consider the Higgs transverse momentum (p_T) distribution in H + 1-jet production for scalar and

TABLE IV. Same as Table III, but for a pseudoscalar Higgs (see Fig. 5).

	σ_{ij}/pb for H + 2-jet (pseudoscalar), WBF cuts		
ij	gg	gq	qq
11	1.42×10^9	2.24×10^9	8.29×10^8
12	-2.11×10^{13}	-6.66×10^{13}	-4.41×10^{13}
13	-7.12×10^{11}	-7.57×10^{11}	$\cdots$
14	$\cdots$	$\cdots$	$\cdots$
15	-4.43×10^{11}	-1.68×10^{13}	-1.55×10^{13}

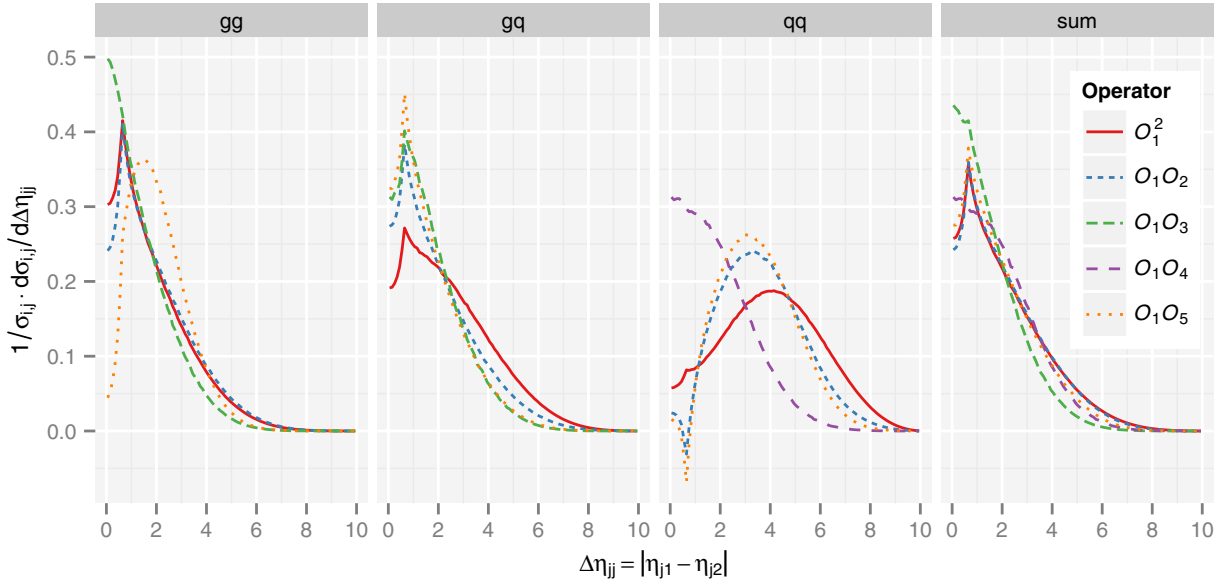

FIG. 6 (color online). Normalized distributions for rapidity separation of the two final state jets for scalar operators. The σ_{ij} are given in Table V.

pseudoscalar Higgs bosons in Figs. 1 and 2. In both cases, one observes large differences in the p_T shape of the individual terms. For comparison, we show the curve that corresponds to SM-like Higgs production through a top loop, obtained from the program SUSHI [25] (curves denoted "SM" for the scalar and "top-loop" for the pseudoscalar). Note, however, that strictly speaking the latter receives an additional p_T dependence through its proportionality to $\alpha_s^2(\mu)$, with $\mu = \sqrt{m_H^2 + p_T^2}$. To properly compare to the predictions from the effective theory, we have divided the SM and top-loop distribution by this factor.

The panel named "sum" in Figs. 1 and 2 shows the sum over the partonic channels for fixed ij. The respective inclusive cross sections to which these curves are normalized are listed in Tables I and II.

As a check, we used these results and combined them with the SM Wilson coefficients of Eq. (4) in order to reproduce the first two nonvanishing terms in the $1/m_t$ expansion for the p_T distribution. The results are shown in Fig. 3. They give some deeper insight into the observations of Ref. [26]. For the gg channel, the interference terms of $\mathcal{O}_1$ with the higher order operators have a very similar shape as the dominant $\mathcal{O}_1\mathcal{O}_1^\dagger$ contribution. The effective

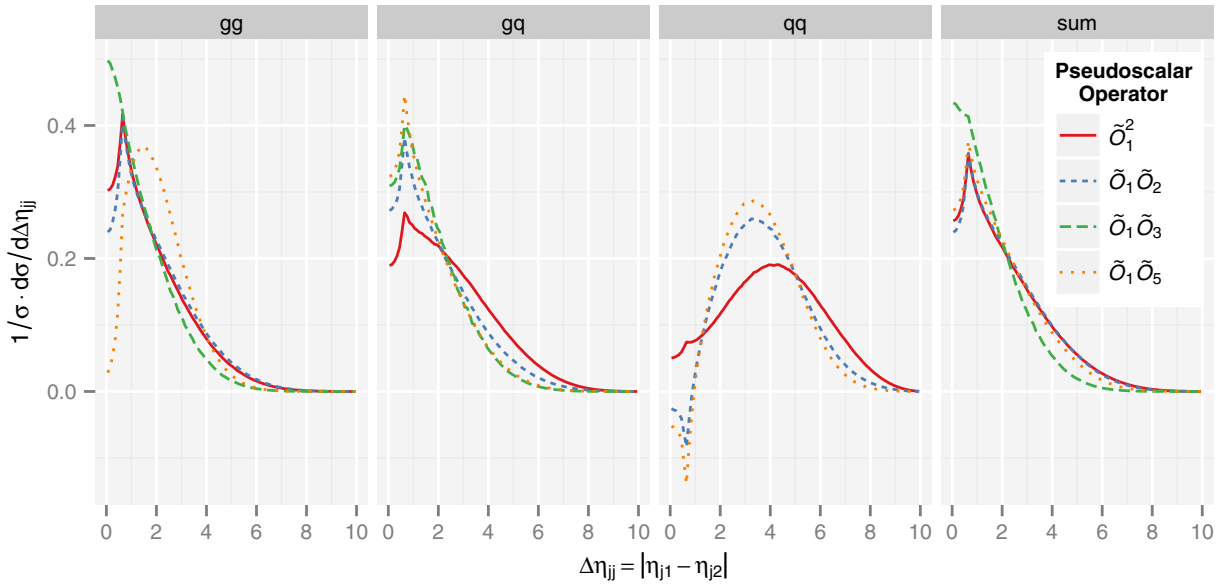

FIG. 7 (color online). Same as Fig. 6, but for pseudoscalar operators. The σ_{ij} are given in Table VI.

TABLE V. Normalization factors for $\Delta\eta_{jj}$ distributions in H + 2-jet production for a scalar Higgs. They are obtained by integrating the distributions of Fig. 6 over the interval $\Delta\eta_{jj} \in [0, 10]$, with the cuts described in Eqs. (9).

	σ_{ij}/pb for H + 2-jet (scalar), incl. cuts		
ij	gg	gq	qq
11	5.00×10^{10}	2.67×10^{10}	2.50×10^{9}
12	-6.41×10^{14}	-1.05×10^{15}	-1.48×10^{14}
13	-6.11×10^{13}	-3.11×10^{13}	...
14	...	...	-1.71×10^{13}
15	-1.42×10^{13}	-3.59×10^{14}	-5.51×10^{13}

TABLE VI. Same as Table V, but for a pseudoscalar Higgs (see Fig. 7).

	σ_{ij}/pb for H + 2-jet (pseudoscalar), incl. cuts		
ij	gg	gq	qq
11	4.94×10^{10}	2.62×10^{10}	2.39×10^{9}
12	-6.32×10^{14}	-1.07×10^{15}	-1.31×10^{14}
13	-6.11×10^{13}	-3.11×10^{13}	...
14	...	...	...
15	-1.36×10^{13}	-3.70×10^{14}	-4.74×10^{13}

theory approach to Higgs production in the SM therefore works extremely well for the gg subchannel, as observed also at NLO QCD in Ref. [26]. For the gq channel, on the other hand, the various contributions differ rather strongly among each other. The $\mathcal{O}_1\mathcal{O}_5^\dagger$ term is even negative; since its magnitude hardly decreases toward larger p_T, it drives the gq channel to negative values. But note that, in contrast to Fig. 1, the scale Λ enters these results, and that it is set to $\Lambda = m_t$; the higher dimensional operators therefore become numerically dominant at $p_T \gtrsim m_t$.

In contrast to the p_T distribution, we do not observe any significant differences for the rapidity distributions among the operators, which is why we refrain from showing these results here.

B. H + 2-jet cross sections

For two jets there are considerably more interesting observables than for the 1-jet case. In particular the azimuthal angle difference $\Delta\Phi_{jj}$ between the two jets and the rapidity separation $\Delta\eta_{jj}$ are well known 2-jet observables for gluon fusion and weak boson fusion (WBF) [27–30]. For example, suitable cuts in $\Delta\Phi_{jj}$ distributions allow one to discriminate a scalar from a pseudoscalar Higgs boson in H + 2-jet production [31]. Also, $\Delta\Phi_{jj}$ and $\Delta\eta_{jj}$ have been proposed to distinguish H + 2-jet production through gluon fusion from WBF [28]. We will study these distributions for the higher dimensional operators of Sec. II and see how they may affect the conclusions drawn from previous studies.

In the following we will use "inclusive" cuts for the $\Delta\eta_{jj}$ distribution,

$$p_{j\perp} > 20 \text{ GeV}, \qquad |\eta_j| < 5, \qquad R_{jj} > 0.6, \tag{9}$$

where $R_{jj} = \sqrt{(\Delta\eta_j)^2 + (\Delta\Phi_{jj})^2}$, and additional "WBF cuts"

$$\begin{aligned} \Delta\eta_{jj} &= |\eta_{j1} - \eta_{j2}| > 4.2, \\ \eta_{j1} \cdot \eta_{j2} &< 0, \qquad m_{jj} > 600 \text{ GeV} \end{aligned} \tag{10}$$

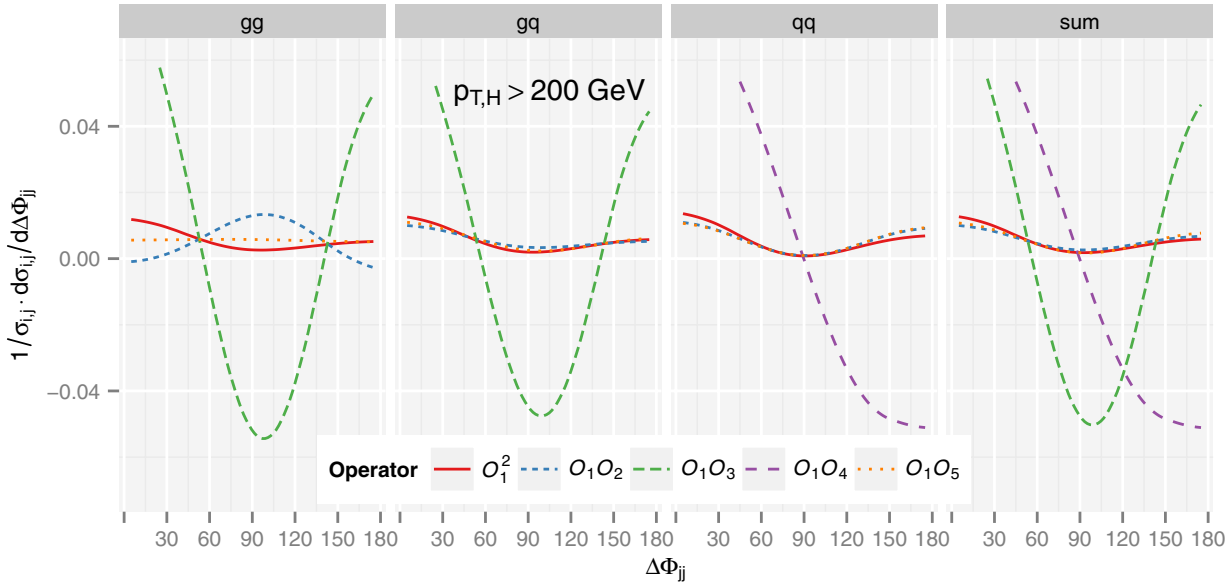

FIG. 8 (color online). Similar to Fig. 4, but restricted to events with $p_T > 200$ GeV, where p_T is the transverse momentum of the Higgs boson. The σ_{ij} are given in Table VII.

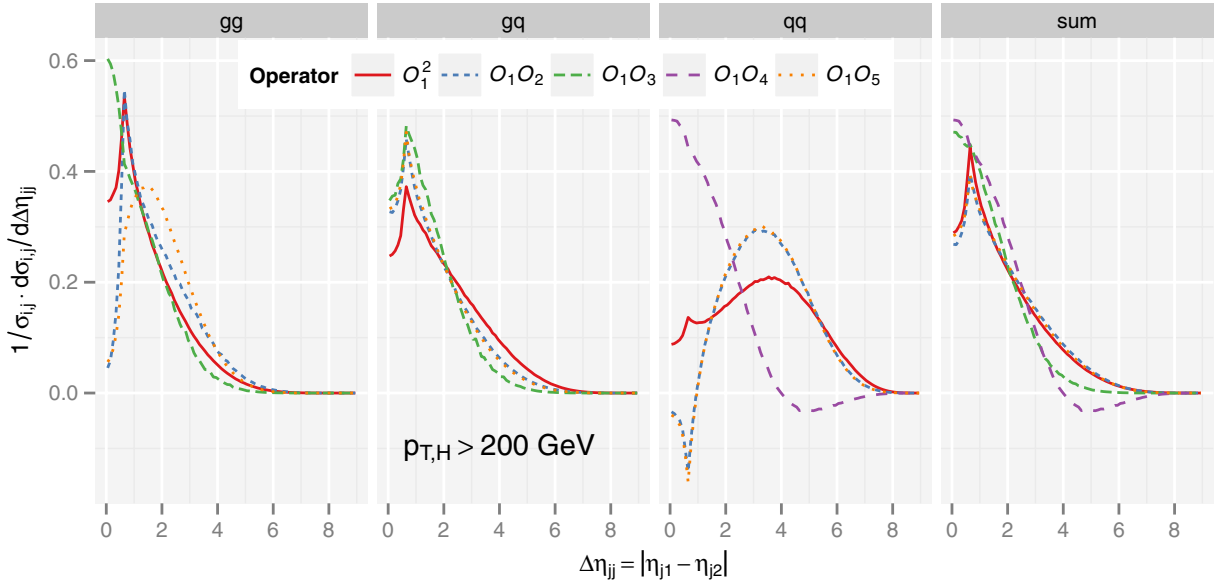

FIG. 9 (color online). Similar to Fig. 6, but restricted to events with $p_T > 200$ GeV, where p_T is the transverse momentum of the Higgs boson. The σ_{ij} are given in Table VIII.

for the $\Delta\Phi_{jj}$ distribution, where m_{jj} is the invariant mass of the two jets.

The $\Delta\Phi_{jj}$ distributions are shown in Figs. 4 and 5. The red curve, corresponding to the contribution from $\mathcal{O}_1\mathcal{O}_1^\dagger$ ($\tilde{\mathcal{O}}_1\tilde{\mathcal{O}}_1^\dagger$), reproduces the results of Ref. [31]. In the scalar as well as in the pseudoscalar case the $\mathcal{O}_3$ ($\tilde{\mathcal{O}}_3$) induced term has a much stronger variation than the formally leading $\mathcal{O}_1\mathcal{O}_1^\dagger$ and the interference terms $\mathcal{O}_1\mathcal{O}_2^\dagger$ and $\mathcal{O}_1\mathcal{O}_5^\dagger$ (respectively, the corresponding pseudoscalar terms). In the scalar case, the "4-quark-operator" $\mathcal{O}_4$ leads to a remarkable deviation from the other terms. As before, "sum" refers to the sum over the partonic subchannels for fixed ij.

Using VBFNLO [32–34], we calculated the $\Delta\Phi_{jj}$ distributions for top-loop induced Higgs production. We find that they hardly differ from the results for $\mathcal{O}_1^\dagger\mathcal{O}_1$ (respectively, $\tilde{\mathcal{O}}_1^\dagger\tilde{\mathcal{O}}_1$) and therefore refrain from including them in our plots.

An explanation for the different curvatures of the leading scalar and pseudoscalar operators $\mathcal{O}_1$ and $\tilde{\mathcal{O}}_1$, i.e. the suppression of planar events for CP-odd couplings, is that

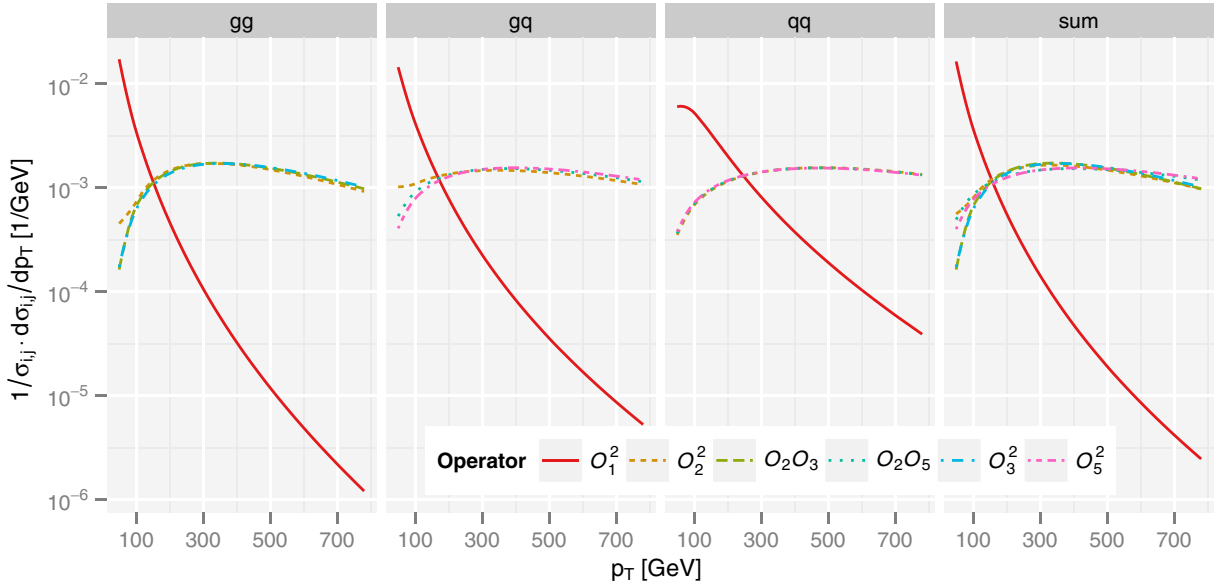

FIG. 10 (color online). Normalized Higgs transverse momentum distributions for scalar coupling operators. The σ_{ij} are given in Table IX.

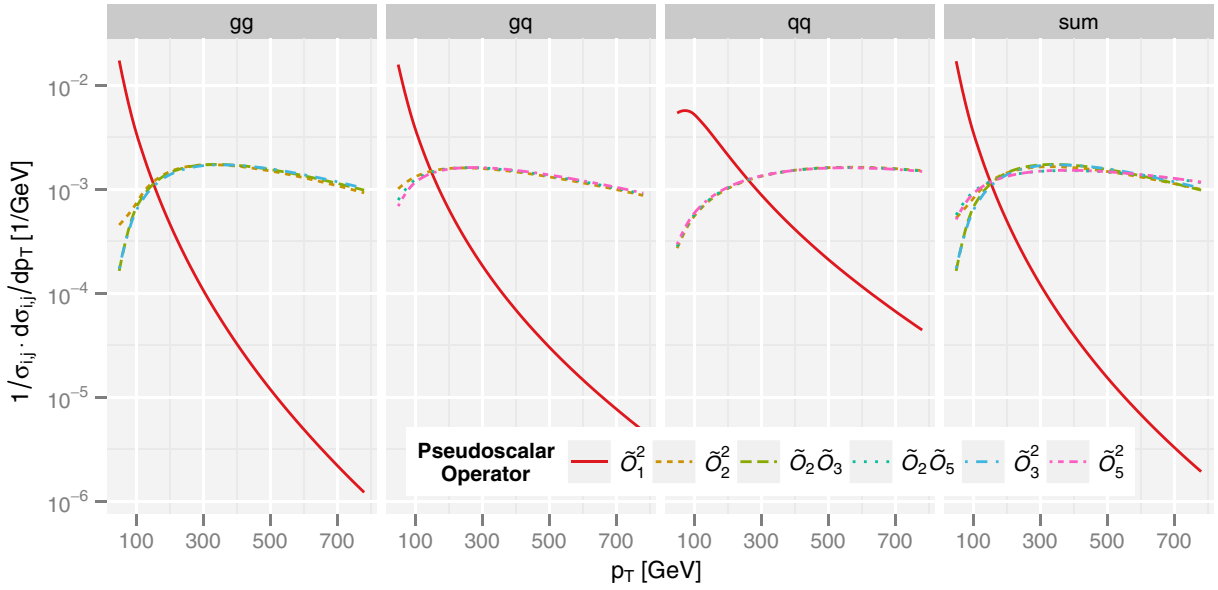

FIG. 11 (color online). Normalized Higgs transverse momentum distributions for pseudoscalar coupling operators. Note that the gg channel is identical to the scalar case. The σ_{ij} are given in Table X.

the epsilon tensor contracted with (four) linearly dependent momentum vectors of the incoming and outgoing partons vanishes [31].

To allow the reader to derive quantitative results for particular models corresponding to specific values for the Wilson coefficients, we provide again in Tables III and IV the integrated cross sections derived with the inclusive plus WBF cuts described in Eqs. (9) and (10).

Distributions for the jet rapidity separation for scalar and pseudoscalar operators are shown in Figs. 6 and 7. The used normalization factors are given in Tables V and VI. One can compare these with the results of [[28], Fig. 8], where the specifics for the $\Delta\eta_{jj}$ distribution for 2-jet gluon-fusion and 2-jet weak boson fusion are discussed: while gluon fusion exhibits a peak at small $\Delta\eta_{jj}$ (due to the

TABLE VII. Normalization factors for $\Delta\Phi_{jj}$ distributions in H + 2-jet production for a scalar Higgs with $p_T > 200$ GeV. They are obtained by integrating the distributions of Fig. 8 over the interval $\Delta\Phi_{jj} \in [0, \pi]$, with the cuts described in Eqs. (9) and (10).

σ_{ij}/pb for H + 2-jet (scalar), WBF cuts $p_{T,H} > 200$ GeV			
ij	gg	gq	qq
11	1.14×10^8	2.36×10^8	1.23×10^8
12	-1.91×10^{12}	-2.32×10^{13}	-2.25×10^{13}
13	-1.28×10^{11}	-1.93×10^{11}	⋯
14	⋯	⋯	3.82×10^{11}
15	-2.34×10^{11}	-1.00×10^{13}	-1.03×10^{13}

TABLE VIII. Normalization factors for $\Delta\eta_{jj}$ distributions in H + 2-jet production for a scalar Higgs with $p_T > 200$ GeV. They are obtained by integrating the distributions of Fig. 6 over the interval $\Delta\eta_{jj} \in [0, 10]$, with the cuts described in Eq. (9).

σ_{ij}/pb for H + 2-jet (scalar), incl. cuts $p_{T,H} > 200$ GeV			
ij	gg	gq	qq
11	3.58×10^9	2.95×10^9	3.84×10^8
12	-3.83×10^{13}	-5.05×10^{14}	-7.00×10^{13}
13	-1.21×10^{13}	-1.30×10^{13}	⋯
14	⋯	⋯	-6.14×10^{12}
15	-6.57×10^{12}	-2.46×10^{14}	-3.23×10^{13}

TABLE IX. Normalization factors for p_T distributions in H + 1-jet production induced by higher dimensional operators for a scalar Higgs (see Fig. 10).

σ_{ij}/pb for H + 1-jet (scalar)			
ij	gg	gq	qq
22	1.35×10^{20}	3.60×10^{19}	1.00×10^{19}
23	-1.12×10^{20}	⋯	⋯
25	⋯	3.35×10^{19}	1.01×10^{19}
33	2.38×10^{19}	⋯	⋯
55	⋯	7.97×10^{18}	2.57×10^{18}

TABLE X. Same as Table IX, but for a pseudoscalar Higgs (see Fig. 11).

σ_{ij}/pb for H + 1-jet (pseudoscalar)			
ij	gg	gq	qq
22	1.35×10^{20}	3.61×10^{19}	2.67×10^{19}
23	-1.12×10^{20}	⋯	⋯
25	⋯	3.48×10^{19}	2.71×10^{19}
33	2.38×10^{19}	⋯	⋯
55	⋯	8.47×10^{18}	6.87×10^{18}

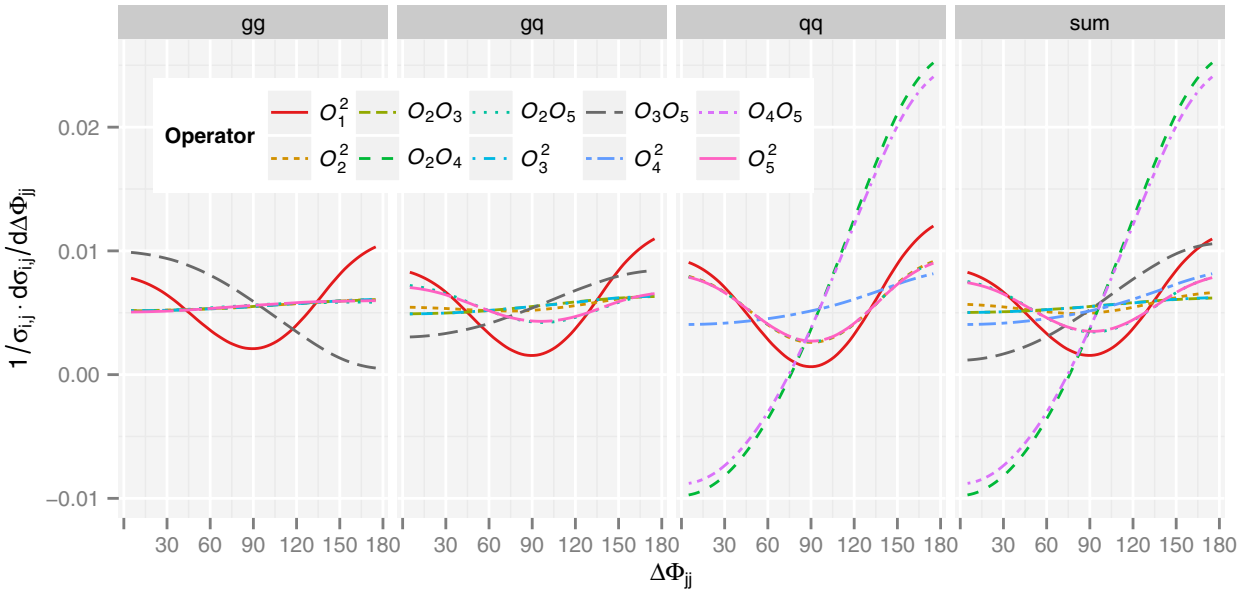

FIG. 12 (color online). Normalized distributions for azimuthal angle difference of the two final state jets for scalar operators. The σ_{ij} are given in Table XI.

jet radius constraint $R_{jj} > 0.6$), for weak boson fusion the peak is at a rapidity separation $\Delta\eta_{jj} \approx 5$ and considerably smaller. We compared our results again to top-loop induced Higgs production obtained with VBFNLO [32–34]; similar to the $\Delta\Phi_{jj}$ distribution, we find that they are almost identical to the curves for $\mathcal{O}_1^\dagger\mathcal{O}_1$ (respectively, $\tilde{\mathcal{O}}_1^\dagger\tilde{\mathcal{O}}_1$), which is why we refrain from including them in our plots.

While there are quantitative differences among the various contributions for the scalar and pseudoscalar operators considered here, we conclude that the qualitative differences are probably too small to be used in an experimental analysis in order to classify the gluon-Higgs coupling.

In light of the fact that the differences among the various operators increase with the Higgs transverse momentum (see Figs. 1 and 2), it is suggestive to consider the $\Delta\Phi_{jj}$ and $\Delta\eta_{jj}$ distributions for these high-p_T events only. For example, Figs. 8 and 9 show these distributions in the scalar Higgs case, when the Higgs' transverse

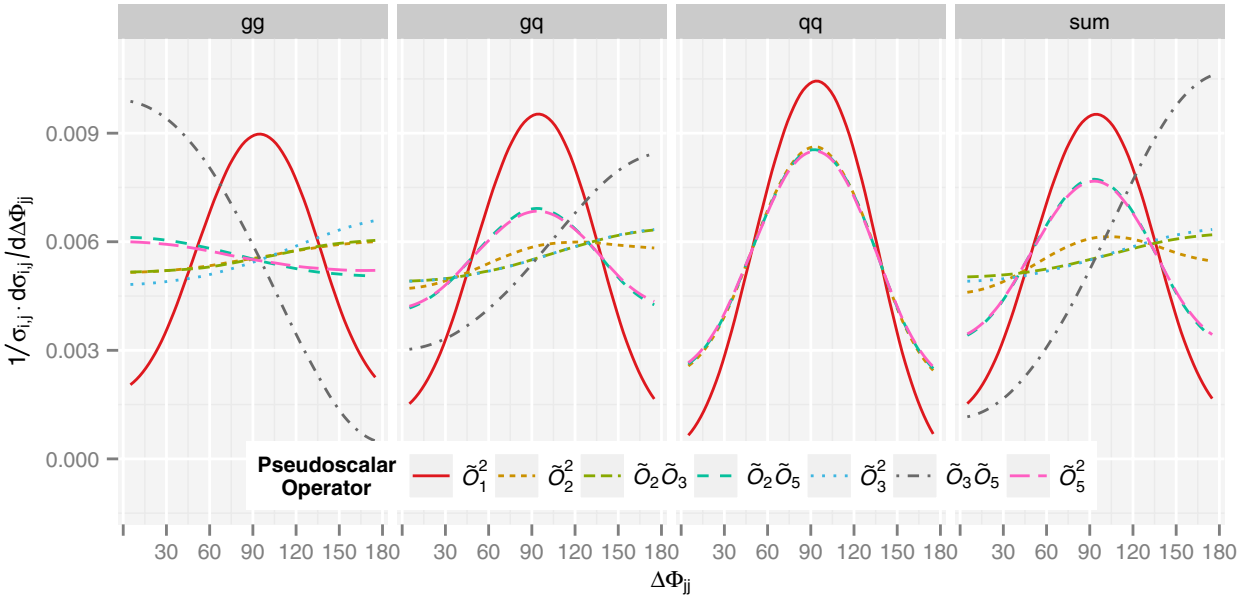

FIG. 13 (color online). Normalized distributions for azimuthal angle difference of the two final state jets for pseudoscalar operators. The σ_{ij} are given in Table XII.

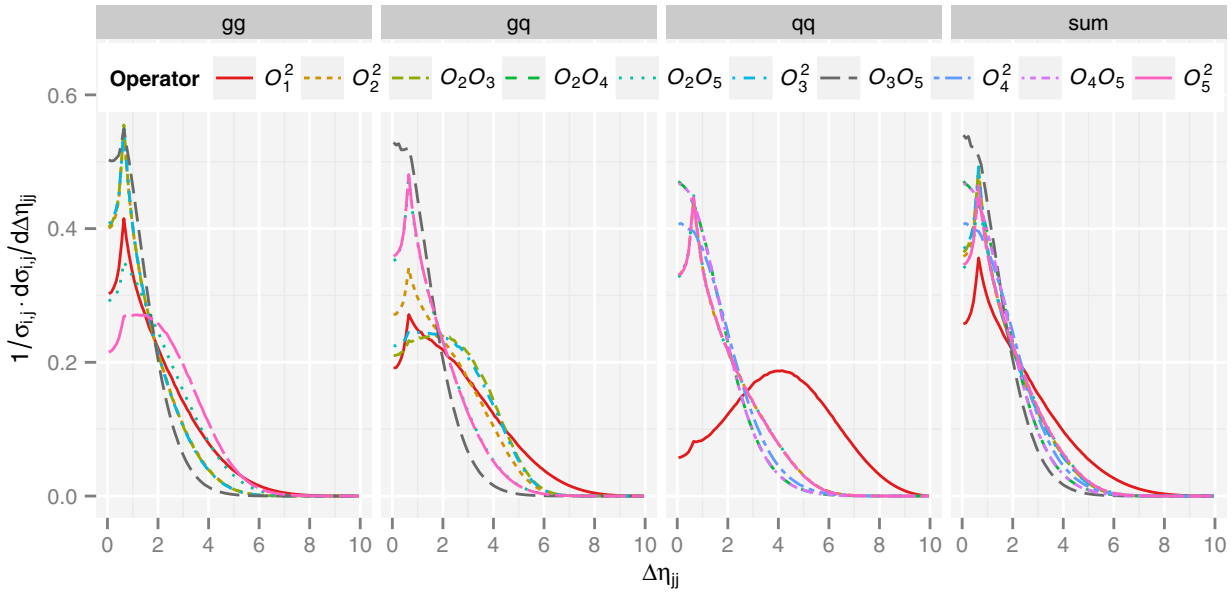

FIG. 14 (color online). Normalized distributions for rapidity separation of the two final state jets for scalar operators. The σ_{ij} are given in Table XIII.

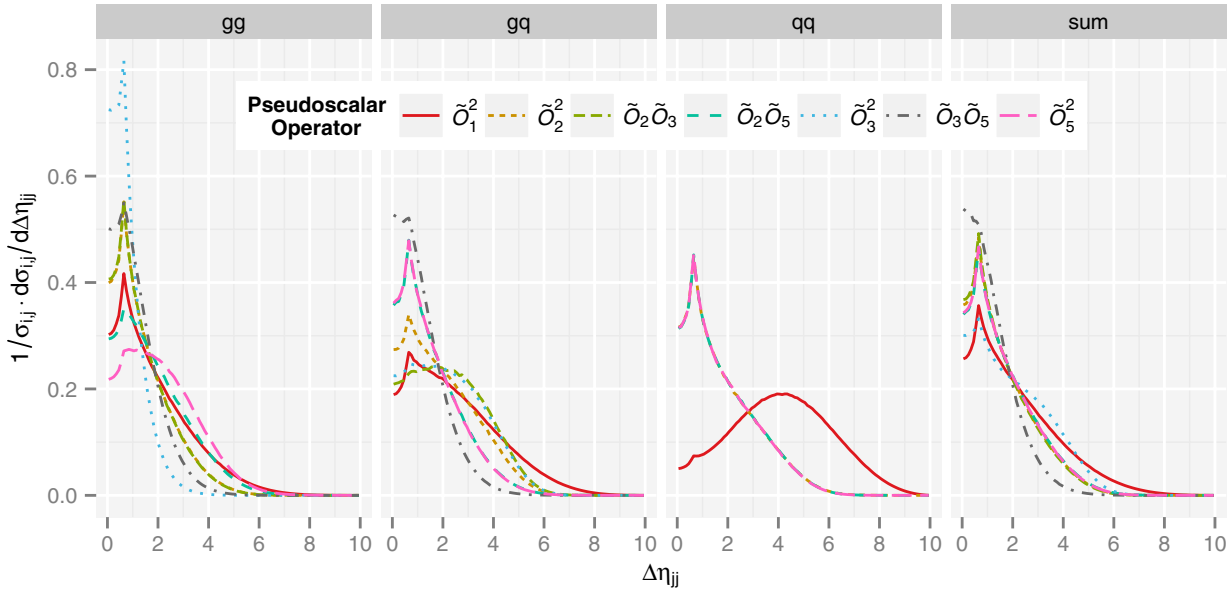

FIG. 15 (color online). Normalized distributions for rapidity separation of the two final state jets for pseudoscalar operators. The σ_{ij} are given in Table XIV.

momentum is restricted to $p_T > 200$ GeV. Compared to Fig. 4, some of the features are strongly enhanced[3]; however, considering the fact that such a cut will significantly decrease the data sample, it remains to be seen whether it would lead to an improvement of an experimental analysis.

[3]The fact that the slope of "$\mathcal{O}_1\mathcal{O}_4$" changes sign is due to a change of sign in the normalization; see Table VII.

IV. HIGHER ORDER SUPPRESSED TERMS

Up to this point, we considered the Lagrangians in Eq. (1) and (6) as an effective theory truncated at $\mathcal{O}(1/\Lambda^3)$. Therefore, we only took into account the square of $\mathcal{O}_1$ (or $\tilde{\mathcal{O}}_1$) and its interference with $\mathcal{O}_n$ (or $\tilde{\mathcal{O}}_n$) ($n \geq 2$), as other terms are of higher order in $1/\Lambda$. In this section, we will consider products of the $\mathcal{O}_n$ (and $\tilde{\mathcal{O}}_n$) ($n \geq 2$) with each other. They might be relevant if indeed the gluon-Higgs coupling is predominantly mediated by one

TABLE XI. Normalization factors for $\Delta\Phi_{jj}$ distributions in H + 2-jet production induced by higher dimensional operators for a scalar Higgs (see Fig. 12).

	σ_{ij}/pb for H + 2-jet (scalar), WBF cuts		
ij	gg	gq	qq
22	1.40×10^{19}	2.01×10^{19}	5.14×10^{18}
23	-1.07×10^{19}	-1.24×10^{19}	⋯
24	⋯	⋯	3.09×10^{17}
25	2.28×10^{17}	4.17×10^{18}	4.96×10^{18}
33	2.08×10^{18}	2.45×10^{18}	⋯
34	⋯	⋯	⋯
35	-2.06×10^{15}	9.60×10^{15}	⋯
44	⋯	⋯	1.20×10^{17}
45	⋯	⋯	1.49×10^{17}
55	5.48×10^{16}	1.02×10^{18}	1.21×10^{18}

TABLE XII. Same as Table XI, but for a pseudoscalar Higgs (see Fig. 13).

	σ_{ij}/pb for H + 2-jet (pseudoscalar), WBF cuts		
ij	gg	gq	qq
22	1.40×10^{19}	2.01×10^{19}	4.88×10^{18}
23	-1.07×10^{19}	-1.24×10^{19}	⋯
24	⋯	⋯	⋯
25	2.28×10^{17}	4.12×10^{18}	4.71×10^{18}
33	2.26×10^{15}	2.45×10^{18}	⋯
34	⋯	⋯	⋯
35	-2.06×10^{15}	9.62×10^{15}	⋯
44	⋯	⋯	⋯
45	⋯	⋯	⋯
55	5.49×10^{16}	1.01×10^{18}	1.15×10^{18}

TABLE XIII. Normalization factors for $\Delta\eta_{jj}$ distributions in H + 2-jet production induced by higher dimensional operators for a scalar Higgs (see Fig. 14).

	σ_{ij}/pb for H + 2-jet (scalar), incl. cuts		
ij	gg	gq	qq
22	7.10×10^{20}	3.10×10^{20}	9.56×10^{19}
23	-5.62×10^{20}	-1.36×10^{20}	⋯
24	⋯	⋯	1.69×10^{19}
25	4.21×10^{18}	1.38×10^{20}	9.38×10^{19}
33	1.12×10^{20}	2.86×10^{19}	⋯
34	⋯	⋯	⋯
35	-4.94×10^{17}	1.65×10^{18}	⋯
44	⋯	⋯	4.26×10^{18}
45	⋯	⋯	8.37×10^{18}
55	7.18×10^{17}	3.49×10^{19}	2.32×10^{19}

TABLE XIV. Same as Table XIII, but for a pseudoscalar Higgs (see Fig. 15).

	σ_{ij}/pb for H + 2-jet (pseudoscalar), incl. cuts		
ij	gg	gq	qq
22	7.11×10^{20}	3.10×10^{20}	8.33×10^{19}
23	-5.62×10^{20}	-1.37×10^{20}	⋯
24	⋯	⋯	⋯
25	4.19×10^{18}	1.39×10^{20}	8.15×10^{19}
33	5.12×10^{18}	2.86×10^{19}	⋯
34	⋯	⋯	⋯
35	-4.94×10^{17}	1.65×10^{18}	⋯
44	⋯	⋯	⋯
45	⋯	⋯	⋯
55	7.15×10^{17}	3.50×10^{19}	2.01×10^{19}

of the dimension-7 operators, as hypothesized in the Introduction. This hypothesis is also the reason why we do not include interference terms of $\mathcal{O}_1$ with dimension-9 operators in this section, as it would be required if we were dealing with a regular analysis at fixed order in $1/\Lambda$.

Figures 10 and 11 show the p_T distributions in the H + 1-jet case as induced by the higher order operators. For comparison, we also include the formally leading term arising from $\mathcal{O}_1\mathcal{O}_1^\dagger$. Two observations in these figures are remarkable: on the one hand, the difference between the shapes of the higher order terms and this formally leading term is quite significant. On the other hand, the higher order terms themselves are all very close to each other. Also, the behavior is very similar in the scalar and the pseudoscalar cases.

The normalizations for the individual curves are given in Tables IX and X.

Similarly, we consider the $\Delta\Phi_{jj}$ distributions for the higher dimensional operators in Figs. 12 and 13, and the $\Delta\eta_{jj}$ distributions in Figs. 14 and 15. While there are quite large qualitative differences in the various $\Delta\Phi_{jj}$ distributions, they are far less prominent in the $\Delta\eta_{jj}$ shapes. The formally leading term induced by $\mathcal{O}_1\mathcal{O}_1^\dagger$ (and $\tilde{\mathcal{O}}_1\tilde{\mathcal{O}}_1^\dagger$) is again included for comparison.

The corresponding normalization factors are given in Tables XI, XII, XIII, and XIV.

V. CONCLUSIONS

In this paper we have studied the influence of higher dimensional operators that couple gluons to a scalar or a pseudoscalar particle H on distributions in H + 1-jet and H + 2-jet production. While the SM assumes a (mostly) top-loop induced gluon-Higgs coupling, an analysis along the lines of our paper will be necessary in order to fully test this hypothesis. We have found that dimension-7 operators significantly affect the p_T distribution of the Higgs boson, leading to a much harder spectrum than in the SM. Also 2-jet observables can be quite sensitive to these effects that are formally subleading in the scale of "new physics."

We note that since, to our knowledge, this is the first analysis of this kind, we have restricted ourselves to the lowest order of perturbation theory. This is certainly justified since experimental measurements of the observables discussed in this paper have only just begun and still carry large uncertainties [35]. However, if deviations relative to the SM predictions are experimentally observed, it will be necessary and interesting to perform the analysis of this paper at NLO QCD.

ACKNOWLEDGMENTS

We would like to thank D. Zeppenfeld for comments on the manuscript and calling our attention to Ref. [15], which considers the effect of dimension-7 operators on SM Higgs production. Further thanks go to H. Mantler for valuable help with the SM predictions. This work was supported by BMBF, Contract No. 05H12PXE.

APPENDIX: NORMALIZATION FACTORS

In this Appendix, we collect the normalization factors for the distributions calculated in this paper. They should allow the reader to reconstruct the absolute distributions for any particular model with specific values of the Wilson coefficients C_i or $\tilde{C}_i$; see Eqs. (1) and (6). Specifically, absolute cross sections $\mathrm{d}\sigma_{ij}$ in picobarns are obtained by multiplying the numbers for $\mathrm{d}\sigma_{ij}/\sigma_{ij}$ read off from the figures in Secs. III and IV by the normalization factors σ_{ij} given in Tables I, II, III, IV, V, VI, VII, VIII, IX, X, XI, XII, XIII, and XIV, times $\mathrm{Re}(C_i^\dagger C_j)/(\Lambda/\mathrm{GeV})^{(n_i+n_j)}$, where $n_1 = 1$ and $n_i = 3$ for $i \neq 1$.[4] In other words, the numbers given here for the σ_{ij} refer to $\Lambda = 1$ GeV and $C_i = 1\ \forall i$.

[4]This factor is not required for the cross sections labeled "SM" or "top-loop," of course.

[1] G. Aad *et al.* (ATLAS Collaboration), Phys. Lett. B **716**, 1 (2012).
[2] S. Chatrchyan *et al.* (CMS Collaboration) Phys. Lett. B **716**, 30 (2012).
[3] S. Heinemeyer *et al.* (LHC Higgs Cross Section Working Group Collaboration), arXiv:1307.1347.
[4] S. Dittmaier *et al.* (LHC Higgs Cross Section Working Group Collaboration), arXiv:1201.3084.
[5] S. Dittmaier *et al.* (LHC Higgs Cross Section Working Group Collaboration) arXiv:1101.0593.
[6] V. Hankele, G. Klämke, D. Zeppenfeld, and T. Figy, Phys. Rev. D **74**, 095001 (2006).
[7] U. Langenegger, M. Spira, A. Starodumov, and P. Trueb, J. High Energy Phys. 06 (2006) 035.
[8] F. Campanario, M. Kubocz, and D. Zeppenfeld, Phys. Rev. D **84**, 095025 (2011).
[9] E. Bagnaschi, G. Degrassi, P. Slavich, and A. Vicini, J. High Energy Phys. 02 (2012) 088.
[10] W. Buchmüller and D. Wyler, Nucl. Phys. **268B**, 621 (1986).
[11] B. Grzadkowski, M. Iskrzynski, M. Misiak, and J. Rosiek, J. High Energy Phys. 10 (2010) 085.
[12] A. David *et al.* (LHC Higgs Cross Section Working Group), arXiv:1209.0040.
[13] J. A. Gracey, Nucl. Phys. **634B**, 192 (2002); **696B**, 295(E) (2004).
[14] D. Neill, arXiv:0908.1573.
[15] J. Germer, Diploma thesis, Universität Karlsruhe, 2007, http://www.itp.kit.edu/prep/diploma/PSFiles/Diplom_Germer.pdf.
[16] K. G. Chetyrkin, J. H. Kühn, and C. Sturm, Nucl. Phys. **744B**, 121 (2006).
[17] Y. Schröder and M. Steinhauser, J. High Energy Phys. 01 (2006) 051.
[18] C. Arzt, Phys. Lett. B **342**, 189 (1995).
[19] H. Georgi, Nucl. Phys. **361B**, 339 (1991).
[20] H. D. Politzer, Nucl. Phys. **172B**, 349 (1980).
[21] A. Semenov, Comput. Phys. Commun. **180**, 431 (2009).
[22] N. D. Christensen and C. Duhr, Comput. Phys. Commun. **180**, 1614 (2009).
[23] M. Tentyukov and J. Fleischer, Comput. Phys. Commun. **132**, 124 (2000).
[24] J. A. Vermaseren, arXiv:math-ph/0010025.
[25] R. V. Harlander, S. Liebler, and H. Mantler, Comput. Phys. Commun. **184**, 1605 (2013).
[26] R. V. Harlander, T. Neumann, K. J. Ozeren, and M. Wiesemann, J. High Energy Phys. 08 (2012) 139.
[27] V. Del Duca, W. Kilgore, C. Oleari, C. R. Schmidt, and D. Zeppenfeld, Phys. Rev. D **67**, 073003 (2003).
[28] V. Del Duca, W. Kilgore, C. Oleari, C. Schmidt, and D. Zeppenfeld, Nucl. Phys. **616B**, 367 (2001).
[29] D. L. Rainwater and D. Zeppenfeld, J. High Energy Phys. 12 (1997) 005.
[30] G. Klämke and D. Zeppenfeld, J. High Energy Phys. 04 (2007) 052.
[31] V. Hankele, G. Klämke, and D. Zeppenfeld, arXiv:hep-ph/0605117.
[32] K. Arnold *et al.*, arXiv:1207.4975.
[33] K. Arnold *et al.*, arXiv:1107.4038.
[34] K. Arnold *et al.*, Comput. Phys. Commun. **180**, 1661 (2009).
[35] ATLAS Collaboration, Report No. ATLAS-CONF-2013-072.